



# Pd nanoparticles immobilized on the magnetic silica–chitosan nanocomposite ( $\text{NiFe}_2\text{O}_4@ \text{SiO}_2@ \text{CS-Pd}$ NPs) promoted the biaryl synthesis

Fatemeh Rafiee<sup>1</sup> · S. Azam Hosseini<sup>1</sup>

Received: 31 October 2018 / Accepted: 5 April 2019  
© Iranian Chemical Society 2019

## Abstract

$\text{NiFe}_2\text{O}_4$  nanoparticles have been prepared by co-precipitation procedure and coated with  $\text{SiO}_2$  following the Stöber process. Then, chitosan was covalently connected with silica to provide an excellent stabilizer and biosupport for the immobilization of Pd nanoparticles. This magnetic bionanocatalyst was characterized by Fourier transform infrared spectroscopy, field-emission scanning electron microscope, transmission electron microscope, energy-dispersive X-ray, X-ray powder detection, vibrating sample magnetometer, inductively coupled plasma atomic emission spectroscopy techniques and CHN analysis. The  $\text{NiFe}_2\text{O}_4@ \text{SiO}_2@ \text{CS-Pd}$  NPs exhibited high activity for the Suzuki coupling reactions of various aryl halides with arylboronic acids. Moreover, this catalyst could be recovered magnetically and recycled for nine times without significant loss of its activity.

**Keywords** Biomaterial supported catalysts · Chitosan · Magnetic nanoparticle support · Heterogeneous catalysts · Magnetic separation · Biphenyls

## Introduction

The natural biopolymers such as cellulose, chitin, chitosan and starch are widely applied as a biosupport due to the availability, non-toxicity, biodegradability, renewability and biocompatibility properties [1–3]. Among them, chitosan was considered to be an ideal support for the immobilization of catalytic metals [4–9]. The presence of available amine and hydroxyl chelating functional groups in this biopolymer led to the stabilization of metal anions specially palladium and platinum. The highly active immobilized metal catalysts supported on chitosan were used in the hydrogenation and acetalization [10], oxidation [11], cycloaddition [12], oxidative carboxylation of olefins [13] and cross-coupling reactions [14–17].

Nanoparticles can effectively improve the loading and the catalytic efficiency of immobilized catalysts due to their high surface to volume ratios. However, they tend to aggregate

and are difficult to recover from reactions due to their small size. Chitosan is able to reduce metal ions to a zero valent oxidation state while controlling nanoparticle growth, and also it can act as a useful stabilizing polymer for metal nanoparticles such as Ag [18], Au [19], Pd and Pt [20]. Due to the strong affinity of this biopolymer to interact with the metal nanoparticles leaching does not occur as with traditional inorganic supports such as silica, alumina and other metal oxides [21].

The chemical instability, lower surface area, dissolution and lower disperse ability of chitosan are the limiting factors in the use of this biopolymer [5, 22]. The restrictions mentioned were improved in the magnetic functionalized chitosan catalysts. These catalysts have attracted a great research attention especially in biomedical applications. Their most important benefits include the enhancement of the stability in solution, improvement of the adsorption capacity and disperse ability of due to high surface area and surface functional groups and facile magnetic separation [23–25].

Biaryls present a significant interest for the synthesis of biologically active compounds [26], natural products [27], receptor macrocyclic molecules [28], liquid crystal materials [29] and asymmetric catalysts [30]. In view of the

✉ Fatemeh Rafiee  
f.rafi@alzahra.ac.ir

<sup>1</sup> Department of Chemistry, Faculty of Physics-Chemistry, Alzahra University, Vanak, Tehran, Iran

importance of biaryls, a number of effective catalytic methods have been developed for forming these compounds via palladium catalyzed Suzuki–Miyaura cross-coupling reaction of arylboronic acid, boronic ester and arylborane reagents with aryl halides or triflates [31].

The immobilized Pd NPs on ligand-free chitosan [32], or modified chitosan for example thiourea-modified chitosan [14], silica–chitosan [15] and chitosan-g-mPEG hybrid [33], chitosan/cellulose-Pd(II) catalyst [16], functionalized chitosan–pd(II) complexes such as Schiff base [34, 35] and amino acid derivatives [36] and magnetic functionalized chitosan-supported palladium catalyst [37] have been used as efficient catalyst source for the Suzuki cross-coupling.

## Experimentals

### Materials and methods

All reagents and solvents used in this study were commercially available and were purchased from commercial suppliers (Acros, Merck and Aldrich) and used without any additional purification. Chitosan was purchased from Exir, and its molecular weight was 100,000–300,000. FT-IR spectra were recorded using a Bruker Tensor 27 spectrometer within the 400–4000  $\text{cm}^{-1}$  range.  $^1\text{H}$  NMR and  $^{13}\text{C}$  NMR spectra were recorded with a Bruker avance 400 and 100 MHz machine, respectively. XRD pattern of the catalyst was recorded with a PW 3710 X-ray diffractometer (Philips) at room temperature using monochromatic  $\text{Cu K}\alpha$  radiation with a wavelength of  $\lambda = 0.15418$  nm. The peak position and intensity were obtained between  $5^\circ$  and  $80^\circ$  with a rate of  $0.04^\circ \text{ s}^{-1}$ . The morphology of the catalyst was observed using a FE-SEM instrument (HITACHI (S4160) Japan) and TEM (PHILIPS CM30). EDX pattern was recorded using a TESCAN, VEGA 3 LMU instrument. Magnetic susceptibility measurements were carried out using a vibrating sample magnetometer (VSM, MDK Co. Ltd, Iran) with the magnetic field range of between +10,000 and –10,000 Oe at room temperature. Elemental analysis was performed on Eager 300 for EA1112 CHNS instrument.

### Synthesis of nickel ferrite ( $\text{NiFe}_2\text{O}_4$ ) nanoparticles

To prepare  $\text{NiFe}_2\text{O}_4$  nanoparticles by co-precipitation technique, the solutions of metallic salts ( $\text{FeCl}_3 \cdot 6\text{H}_2\text{O}$ , 100 ml, 0.2 M and  $\text{NiCl}_2 \cdot 6\text{H}_2\text{O}$ , 100 ml, 0.1 M) were prepared separately and mixed together. The solution was stirred for an hour. Then, in order for pH to reach 13, a solution of NaOH (~18 ml, 3 M) was added slowly to the flask. Finally, oleic acid (3 drops) was added to the solution as surfactant to prevent the aggregation and agglomeration of the nanoparticles. Then, the suspension was vigorously stirred using

a magnetic stirring bar at  $70^\circ\text{C}$  for 2 h. After complete precipitation, the residue was washed with double distilled water ( $3 \times 25$  ml) and dried in an oven at  $90^\circ\text{C}$  over night; then, it was calcinated at  $600^\circ\text{C}$  for 4 h [38].

### Silica coating process

Coating of these nanoparticles with silica was carried out by ultrasonic dispersion of 0.5 g of  $\text{NiFe}_2\text{O}_4$  nanoparticles in 40 ml ethanol and 4 ml of deionized water. Then, 5 ml ammonium hydroxide (25%) was added to the mixture. After stirring for around 15 min, 2 ml of tetraethyl orthosilicate (TEOS) was added drop by drop to the mixture. The reaction was then allowed to proceed for 30 min in an ultrasonic bath and then continuously stirred at room temperature for 12 h. The silica-coated nanoparticles were collected by an external magnet, followed by washing three times with ethanol and deionized water and then dried in the oven at  $80^\circ\text{C}$  for 12 h [39].

### Chitosan coating process

For the synthesis of chitosan-coated magnetite nanoparticles, amount of 0.5 g of the  $\text{SiO}_2$ -coated  $\text{NiFe}_2\text{O}_4$  nanoparticles were dispersed in chitosan solution (contain 1 g chitosan that dissolved in 40 ml of a 2% acetic acid solution) using an ultrasonic bath for 30 min at  $60^\circ\text{C}$ . The reaction was then allowed to proceed at room temperature under continuous stirring for 12 h. Then, the chitosan-coated  $\text{NiFe}_2\text{O}_4 @ \text{SiO}_2$  nanoparticles were separated by an external magnet and washed several times with ethanol and dried in the oven at  $80^\circ\text{C}$  overnight. This step was done according to the reported process for chitosan coating of magnetite nanoparticles [40].

### Preparation of $\text{NiFe}_2\text{O}_4 @ \text{SiO}_2 @ \text{CS-Pd}$ catalyst

1 g of  $\text{NiFe}_2\text{O}_4 @ \text{SiO}_2 @ \text{CS}$ , 0.02 g (0.12 mmol) of  $\text{PdCl}_2$  and 10 ml of ethanol were placed in a round bottom flask equipped with magnetic stirrer and a reflux condenser. The mixture was stirred and refluxed for 8 h. Then,  $\text{NiFe}_2\text{O}_4 @ \text{SiO}_2 @ \text{CS-Pd}$  nanocomposite was separated by a permanent magnet and washed five times with deionized water and dried in the oven at  $80^\circ\text{C}$  for 10 h.

### General procedure for the Suzuki–Miyaura reaction of aryl halides with arylboronic acids

To a round-bottomed flask containing a mixture of aryl halide (1 mmol), arylboronic acid (1.1 mmol) and  $\text{K}_2\text{CO}_3$  (2 mmol) in 2 ml of EtOH,  $\text{NiFe}_2\text{O}_4 @ \text{SiO}_2 @ \text{CS-Pd}$  catalyst (0.002 g,  $8 \times 10^{-5}$  mol% Pd) was added and stirred at  $75^\circ\text{C}$  for the time specified in Table 2. After completion of the

reaction (monitored by TLC (*n*-hexane/EtOAc, 9: 1) or GC), the reaction mixture was cooled to room temperature and the catalyst was separated by applying an external magnet. Then, the reaction mixture was diluted with water and the resultant mixture extracted with *n*-hexane to isolate the products. The combined organic layers were dried over  $\text{MgSO}_4$ , and the solvent was evaporated under reduced pressure.

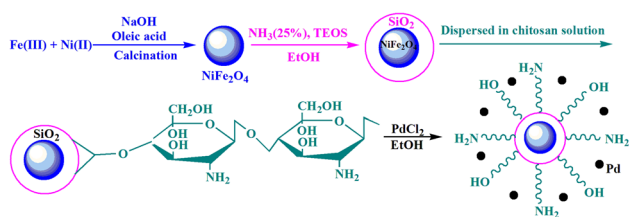
## Result and discussion

### Preparation of $\text{NiFe}_2\text{O}_4@ \text{SiO}_2@ \text{CS-Pd}$ catalyst

Nickel ferrite ( $\text{NiFe}_2\text{O}_4$ ) is one of the most important members of the spinel ferrites, with a particular ferromagnetism quality that have high saturation magnetization, high Curie temperature, chemical stability and relatively high permeability [41–43]. We have already prepared  $\text{NiFe}_2\text{O}_4$  nanoparticles and investigated its catalytic activity in the synthesis of 5-substituted 1H-tetrazoles [44].

The magnetic nanoparticle-supported Pd catalyst ( $\text{NiFe}_2\text{O}_4@ \text{SiO}_2@ \text{CS-Pd}$  NPs) was synthesized via multiple steps. The first step was to prepare  $\text{NiFe}_2\text{O}_4$  nanoparticles from commercial sourced ferric chloride ( $\text{FeCl}_3 \cdot 6\text{H}_2\text{O}$ ) and nickel chloride ( $\text{NiCl}_2 \cdot 6\text{H}_2\text{O}$ ) in proper pH and the presence of oleic acid as a surfactant. Second, the obtained MNPs were subsequently coated with silica ( $\text{NiFe}_2\text{O}_4@ \text{SiO}_2$ ) through the well-known Stöber method with TEOS. The  $\text{NiFe}_2\text{O}_4@ \text{SiO}_2$  core/shell structures are then sequentially treated by chitosan to form  $\text{NiFe}_2\text{O}_4@ \text{SiO}_2@ \text{CS}$ . Finally, Pd nanoparticles were immobilized on this support through the reaction with  $\text{PdCl}_2$  in ethanol that chitosan acted as a stabilizer and reducing agent (Scheme 1).

The surface oxidation and agglomeration of magnetic nanoparticles result in a significant decrease in their magnetic properties, surface area and catalytic activity. Due to the strong surface affinity of the magnetic nanoparticles toward silica as a chemically inert material with high surface area and good stability, it often employed as coating layer material over the surface. This surface modification can weaken the particle–particle magnetic bipolar interactions and protects the nanoparticles from aggregation and



**Scheme 1** Procedure for preparation of  $\text{NiFe}_2\text{O}_4@ \text{SiO}_2@ \text{CS-Pd}$  catalyst

oxidation processes. The organic-silica based polymeric materials having metal chelating ability anchored to the silica surface and offer advantages such as combination of the hardness of silica and polymer functional properties and also enhancement of catalytic centers [15, 45, 46].

### Characterization of $\text{NiFe}_2\text{O}_4@ \text{SiO}_2@ \text{CS-Pd}$

Figure 1 shows the FT-IR spectrum of  $\text{NiFe}_2\text{O}_4$ ,  $\text{NiFe}_2\text{O}_4@ \text{SiO}_2$ , pure chitosan,  $\text{NiFe}_2\text{O}_4@ \text{SiO}_2@ \text{CS}$  and palladium supported on  $\text{NiFe}_2\text{O}_4@ \text{SiO}_2@ \text{CS}$  catalyst. In the spectrum of pure chitosan (Fig. 1a), the characteristic absorption bands appear at 3422 (O–H and N–H stretching vibrations), 2922 (C–H stretching vibrations), 1653 (N–H bending vibration), 1423 (C–N stretching vibrations), 1383 ( $\text{CH}_3$  symmetrical angular deformation) 1150–1100  $\text{cm}^{-1}$  (C–O–C and C–O stretching vibrations). All spinel ferrites have two significant absorption bands in the low-frequency region (1000–400  $\text{cm}^{-1}$ ), the highest and lowest ones. This spectrum (Fig. 1b) demonstrates that the highest band at 651  $\text{cm}^{-1}$  corresponds to the intrinsic stretching vibration of metal–oxygen at the tetrahedral site and the lowest one corresponds to the octahedral metal–oxygen stretching at about 467  $\text{cm}^{-1}$ . The absorption broad bands at 3424 and 1634  $\text{cm}^{-1}$  assigned to OH stretching and bending modes of water. As shown in Fig. 1c, the strong absorption band at 1091  $\text{cm}^{-1}$  is related to Si–O–Si antisymmetric stretching vibrations; the absorption peaks at 796  $\text{cm}^{-1}$  and 473  $\text{cm}^{-1}$  are due to the Si–O–Si symmetric stretching and Si–O–Si or O–Si–O bending mode, respectively. These data confirm the successful coating of silica layers on  $\text{NiFe}_2\text{O}_4$ .

The comparison of the spectra of  $\text{NiFe}_2\text{O}_4@ \text{SiO}_2@ \text{CS}$  with those of pure Chitosan and  $\text{NiFe}_2\text{O}_4@ \text{SiO}_2$  indicates successful immobilization of chitosan on the surface of  $\text{NiFe}_2\text{O}_4@ \text{SiO}_2$  nanoparticles (Fig. 1d).

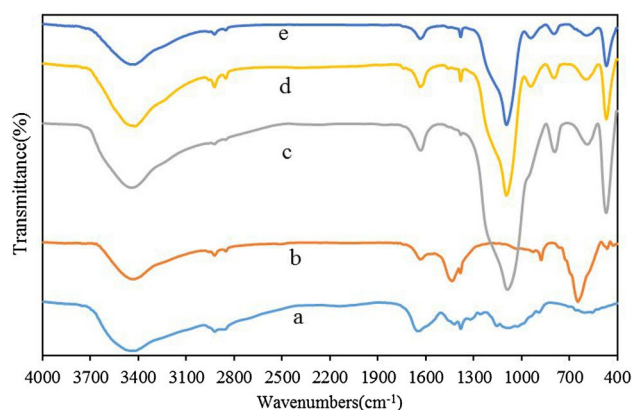


**Fig. 1** FT-IR spectra of chitosan (a),  $\text{NiFe}_2\text{O}_4$  (b),  $\text{NiFe}_2\text{O}_4@ \text{SiO}_2$  (c),  $\text{NiFe}_2\text{O}_4@ \text{SiO}_2@ \text{CS}$  (d),  $\text{NiFe}_2\text{O}_4@ \text{SiO}_2@ \text{CS-Pd}$  (e)

In the powder XRD pattern of the  $\text{NiFe}_2\text{O}_4@\text{SiO}_2@\text{CS-Pd}$  nanocomposite (Fig. 2), the diffraction peaks observed at  $2\theta = 30.71^\circ, 36.18^\circ, 37.93^\circ, 43.99^\circ, 54.35^\circ, 57.89^\circ, 63.44^\circ$  and  $74.80^\circ$  correspond to crystalline planes (220), (311), (222), (400), (422), (511), (440) and (533) of  $\text{NiFe}_2\text{O}_4$  nanoparticles (with the cubic spinel structure), respectively. No diffraction peaks of impurities such as  $\alpha\text{-Fe}_2\text{O}_3$  or NiO and other secondary phases are detected. It is clearly observed that the reflection peaks are sharp and narrow, indicating a high degree of crystallinity and phase purity of the product. Also the XRD pattern of this nanocomposite contains the new characteristic peaks at  $40.09^\circ, 46.68^\circ, 67.93^\circ$  which are indexed, respectively, to the (111), (200) and (220) crystalline planes of Pd nanocrystal suggesting the formation of metallic Pd NPs ( $\text{Pd}^0$ ). The broad peaks appeared from  $18^\circ$  to  $24^\circ$  cover the amorphous silica phase around the magnetic core.

A magnetic measurement of magnetic chitosan nanocomposite was investigated with a vibrating sample magnetometer at room temperature in the applied magnetic field sweeping from  $-10$  to  $10$  kOe (Fig. 3). It can be seen that this catalyst shows ferromagnetic behavior. The saturation magnetization ( $M_s$ ) value for the  $\text{NiFe}_2\text{O}_4@\text{SiO}_2@\text{CS-Pd}$  catalyst ( $11.7 \text{ emu g}^{-1}$ ) is determined to be significantly lower than that of bare  $\text{NiFe}_2\text{O}_4$  that was reported in the literature ( $\sim 40 \text{ emu g}^{-1}$ ). The low magnetic susceptibility of chitosan-coated magnetic nanoparticles arises from a double coating of magnetite core by diamagnetic silica shell and polymeric layer. The magnetic properties of the silica- and polymer-coated samples depend on the  $\text{NiFe}_2\text{O}_4$ . In this sample, there is less magnetic material per gram, and the magnetization readings are divided by substantial mass of silica and chitosan. The other is the non-magnetic coating layer at the surface, affecting the uniformity or magnitude of magnetization due to quenching of surface moments [47]. Even with this reduction in the saturation magnetization, the catalyst can still be separated from the reaction mixture using an external magnetic field.

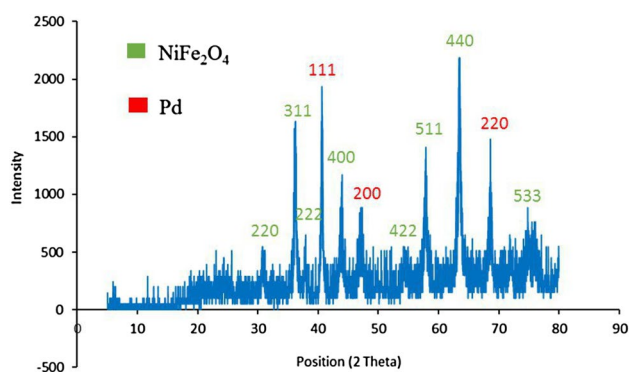


Fig. 2 XRD pattern of  $\text{NiFe}_2\text{O}_4@\text{SiO}_2@\text{CS-Pd}$  nanocomposite

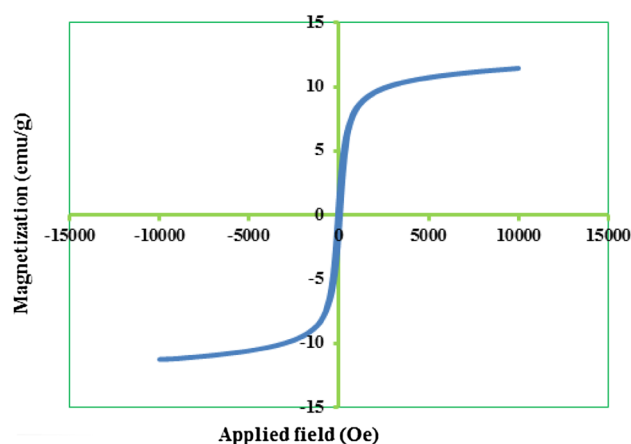


Fig. 3 Room temperature magnetization curve of  $\text{NiFe}_2\text{O}_4@\text{SiO}_2@\text{CS-Pd}$  catalyst

The morphology and size of the nanoparticles were obtained from FE-SEM and TEM analysis. The FE-SEM photograph (Fig. 4) of the nanocomposite demonstrates that the prepared magnetic nanoparticles are spherical in shape with slight agglomeration. TEM images of the catalyst at different magnifications show that Pd nanoparticles are spherical, narrowly distributed and well dispersed in the polymer matrix with average size  $< 10$  nm in diameter.

In the EDX spectrum of the nanocomposite (Fig. 5), the presence of Ni, Fe, Si and O signals indicates that the nickel ferrite nanoparticles are loaded into silica, and the higher intensity of the Si peak compared with the Ni and Fe peaks indicates that the magnetic nanoparticles were trapped by

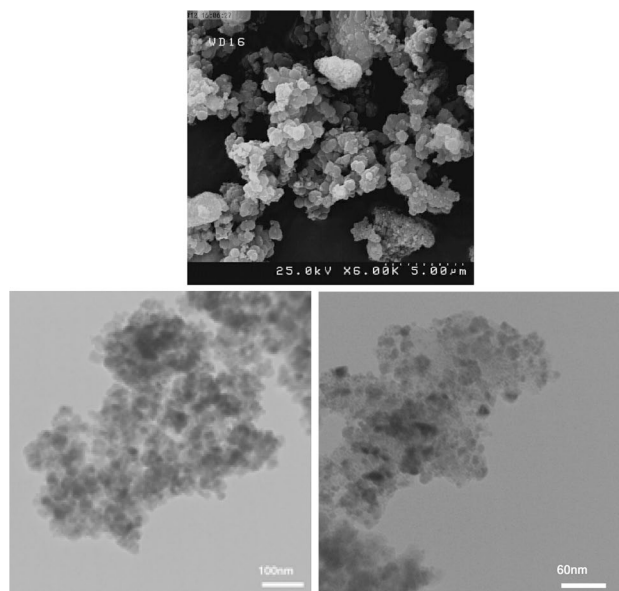


Fig. 4 FE-SEM and TEM images of  $\text{NiFe}_2\text{O}_4@\text{SiO}_2@\text{CS-Pd}$

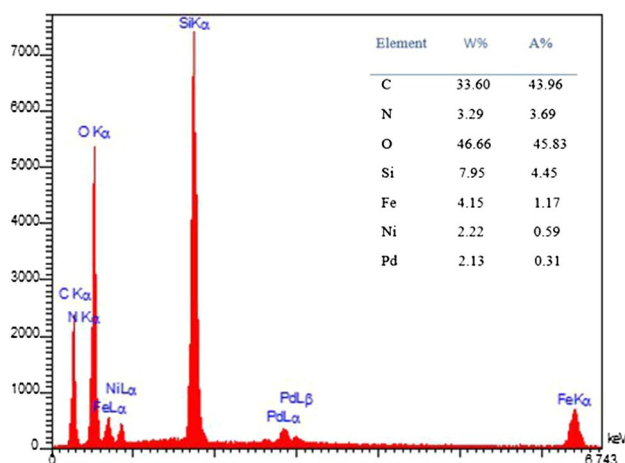


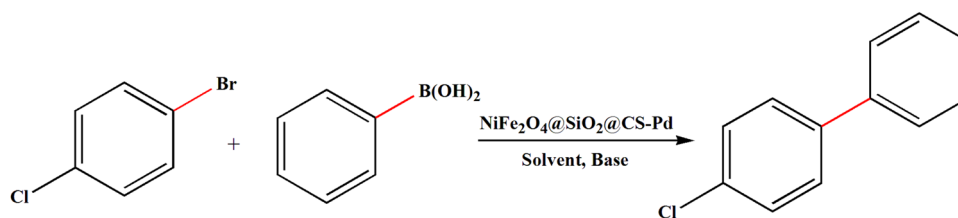
Fig. 5 EDX spectra of NiFe<sub>2</sub>O<sub>4</sub>@SiO<sub>2</sub>@CS-Pd

SiO<sub>2</sub>. Figure 5 also reveals the presence of palladium on the surface of chitosan matrix. The exact amount of palladium in the catalyst as determined by inductively coupled plasma atomic emission spectroscopy (ICP-AES) was 4.2 wt% (0.39 mmol/g). Also the content of carbon, nitrogen and hydrogen is found by CHN analysis to be 10.42, 2.21 and 10.70%, respectively.

### The investigation of catalytic activity of the NiFe<sub>2</sub>O<sub>4</sub>@SiO<sub>2</sub>@CS-Pd in C–C coupling

In 2015, Jadhav et al. [15] reported that in silica–chitosan hybrid material, chitosan (as ligand and support to stabilize palladium) covalently connected with silica. This biopolymer provides a platform to Pd and prevents the removal of palladium from the silica surface.

Table 1 Optimization of reaction conditions for the Suzuki cross-coupling reaction<sup>a</sup>



Entry	Solvent	Base	Catalyst (g)	Temp. (°C)	Conversion (%) <sup>b</sup>
1	H <sub>2</sub> O	K <sub>2</sub> CO <sub>3</sub>	0.005	rt	–
2	H <sub>2</sub> O	K <sub>2</sub> CO <sub>3</sub>	0.005	100	–
3	EtOH	K <sub>2</sub> CO <sub>3</sub>	0.005	rt	90
4	EtOH	K <sub>2</sub> CO <sub>3</sub>	0.005	75	100
5	DMSO	K <sub>2</sub> CO <sub>3</sub>	0.005	Reflux	–
6	DMF	K <sub>2</sub> CO <sub>3</sub>	0.005	Reflux	100
7	Me–Ph	K <sub>2</sub> CO <sub>3</sub>	0.005	110	–
8	MeCN	K <sub>2</sub> CO <sub>3</sub>	0.005	80	50
9	EtOH	NaHCO <sub>3</sub>	0.005	75	80
10	EtOH	NaOAc	0.005	75	–
11	EtOH	Na <sub>2</sub> CO <sub>3</sub>	0.005	75	70
12	EtOH	KOH	0.005	75	90
13	EtOH	KHCO <sub>3</sub>	0.005	75	85
14	EtOH	K <sub>2</sub> CO <sub>3</sub>	–	75	–
15	EtOH	K <sub>2</sub> CO <sub>3</sub>	0.001	75	80
16	EtOH	K <sub>2</sub> CO <sub>3</sub>	0.002	75	100
17	EtOH	K <sub>2</sub> CO <sub>3</sub>	0.003	75	100

<sup>a</sup>Reactions conditions: 1-bromo-4chlorobenzene (1 mmol), phenylboronic acid (1 mmol), base (2 mmol), NiFe<sub>2</sub>O<sub>4</sub>@SiO<sub>2</sub>@CS-Pd nanocatalyst (g), solvent (3.0 ml), 1 h

<sup>b</sup>Determined by GC and TLC

**Table 2** Suzuki cross-coupling reaction using NiFe<sub>2</sub>O<sub>4</sub>@SiO<sub>2</sub>-CS-Pd nanocatalyst

Entry	Ar-X	ArB(OH) <sub>2</sub>	Time (min)	Yield (%) <sup>a</sup>	m.p. (°C)	Refs.
1	Ph-Br	PhB(OH) <sub>2</sub>	5	98	68–70	[48]
2	<i>p</i> -CHO-PhBr	PhB(OH) <sub>2</sub>	30	96	56–58	[49]
3	<i>p</i> -MeOC-Ph-Br	PhB(OH) <sub>2</sub>	45	98	118–120	[48]
4	<i>m</i> -O <sub>2</sub> N-Ph-I	PhB(OH) <sub>2</sub>	30	94	58–60	[50]
5	<i>p</i> -NC-Ph-Br	PhB(OH) <sub>2</sub>	45	97	84–86	[51]
6	<i>p</i> -Cl-Ph-Br	PhB(OH) <sub>2</sub>	15	98	74–76	[48]
7	<i>p</i> -CHO-PhBr	<i>p</i> -Me-PhB(OH) <sub>2</sub>	30	95	104–106	[52]
8	<i>p</i> -NC-Ph-Br	<i>p</i> -Me-PhB(OH) <sub>2</sub>	30	96	109–111	[51]
9	<i>p</i> -Cl-Ph-Br	<i>p</i> -Me-PhB(OH) <sub>2</sub>	15	98	125–127	[51]
10	<i>m</i> -O <sub>2</sub> N-Ph-I	<i>p</i> -Me-PhB(OH) <sub>2</sub>	30	93	76–78	[50]
11	<i>p</i> -NC-Ph-Br	<i>p</i> -Me-PhB(OH) <sub>2</sub>	30	96	109–111	[51]
12	<i>p</i> -Me-Ph-I	<i>p</i> -Me-PhB(OH) <sub>2</sub>	30	95	118–120	[53]
13	<i>p</i> -MeO-Ph-I	<i>p</i> -Me-PhB(OH) <sub>2</sub>	30	94	108–110	[51]
14	<i>p</i> -MeOC-Ph-Br	3,4,5-tri-flouro-PhB(OH) <sub>2</sub>	180	98	119–122	[54]
15	<i>p</i> -CHO-Ph-Br	3,4,5-tri-flouro-PhB(OH) <sub>2</sub>	180	98	109–111	[54]
16	<i>p</i> -MeOC-Ph-Br	<i>m</i> -MeO-PhB(OH) <sub>2</sub>	120	94	48–50	[55]
17	<i>p</i> -MeOC-Ph-Br	<i>p</i> -MeOC-PhB(OH) <sub>2</sub>	120	97	189–190	[53]
18	Ph-Cl	PhB(OH) <sub>2</sub>	180	90	68–70	[48]

Reactions conditions: aryl halide (1 mmol), arylboronic acid (1 mmol), K<sub>2</sub>CO<sub>3</sub> (2 mmol), NiFe<sub>2</sub>O<sub>4</sub>@SiO<sub>2</sub>@CS-Pd nanocatalyst (8 × 10<sup>-5</sup> mol%), ethanol (3.0 ml), 75 °C

<sup>a</sup>Isolated yields

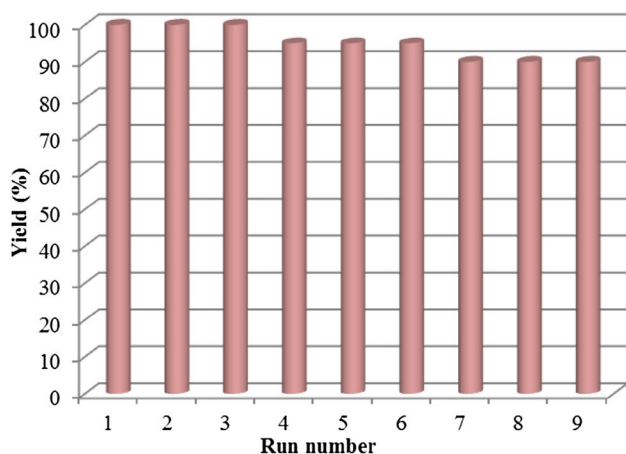


**Fig. 6** Reusability of the NiFe<sub>2</sub>O<sub>4</sub>@SiO<sub>2</sub>@CS-Pd catalyst

In order to show the catalytic activity of synthesized Pd nanocatalyst in the Suzuki–Miyaura coupling reaction, we employed the coupling reaction of 4-bromoanisole with phenylboronic acid as a model reaction to optimize the reaction conditions. The best results were obtained in ethanol as the solvent and K<sub>2</sub>CO<sub>3</sub> as base by employing 0.002 g of nanocatalyst (8 × 10<sup>-5</sup> mol% palladium) at 75 °C. As this catalyst is not sensitive to oxygen, the reactions were carried out under air atmosphere (Table 1).

We then explored the synthesis of various biphenyl derivatives under the optimized conditions, in order to probe the

scope and generality of the process. The results are summarized in Table 2. Both electron-rich and electron-deficient aryl halides and arylboronic acids were superior and delivered products with good to excellent yields. Prolonged reaction time was required for the less active aryl chlorides to obtain a moderate yield. A wide range of functional groups, such as nitryl (NO<sub>2</sub>), nitrile (CN), methyl, methoxy, and carbonyl (COCH<sub>3</sub> and CHO), were tolerated in the reactions.

To study the recyclability of NiFe<sub>2</sub>O<sub>4</sub>@SiO<sub>2</sub>@CS-Pd, we carried out a set of experiments using the recycled catalyst for the Suzuki–Miyaura coupling reaction of 1-bromo-4-chlorobenzene with phenyl boronic acid under optimized conditions. After the completion of the first reaction, the catalyst was recovered magnetically, washed with ethanol and finally dried for the next run. Then, a new reaction was carried out with fresh reactants and solvent under the same conditions. Based on the results, this catalyst could be used at least nine times without any significant loss of its catalytic activity (Fig. 6).

Hot filtration tests of fresh catalyst in the first use and also recycled catalyst showed that coupling conversion was only 40% and no improvement of the product yield observed even in longer times. ICP-AES analysis data showed that the amount of palladium leaching from the surface into the filtrate after catalyst recycling was < 1%.

The chemical structure of the recycled catalyst after the 3 run was investigated by using of FT-IR spectroscopy (Fig. 7) and XRD analysis (Fig. 8). The same diffraction peaks and

**Fig. 7** FT-IR spectra of recycled  $\text{NiFe}_2\text{O}_4@ \text{SiO}_2@ \text{CS-Pd}$  catalyst after the 3 run

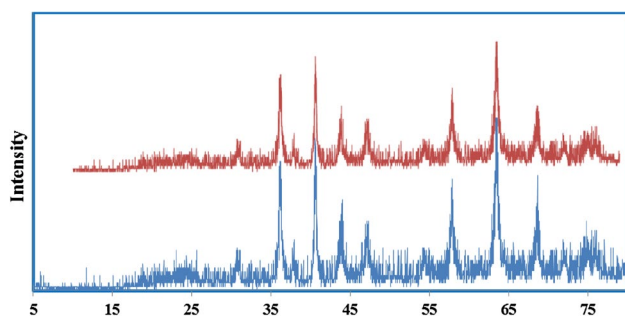
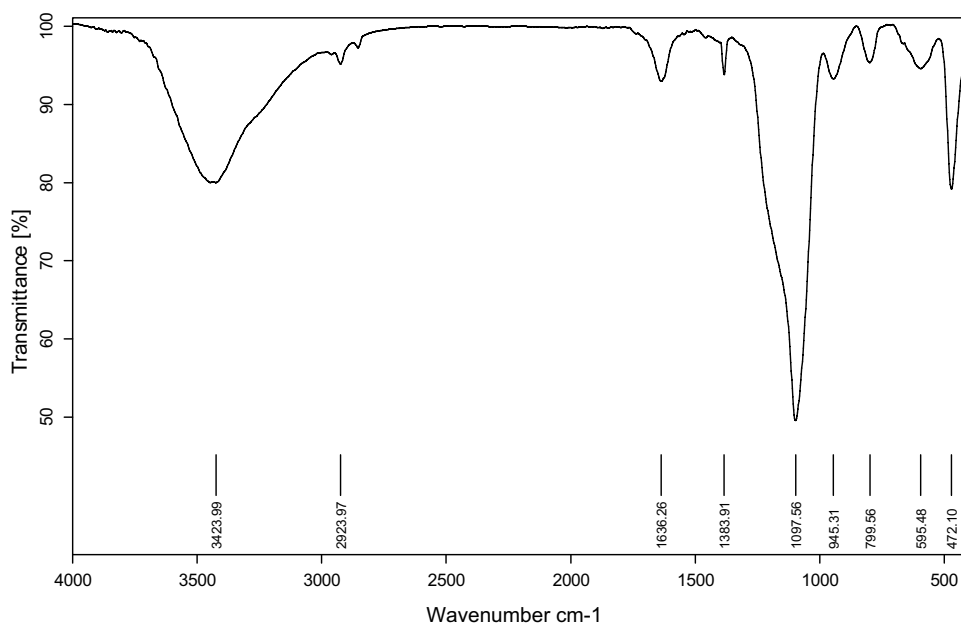


**Fig. 8** XRD pattern of recycled  $\text{NiFe}_2\text{O}_4@ \text{SiO}_2@ \text{CS-Pd}$  catalyst after the 3 run (red) and fresh catalyst (blue)

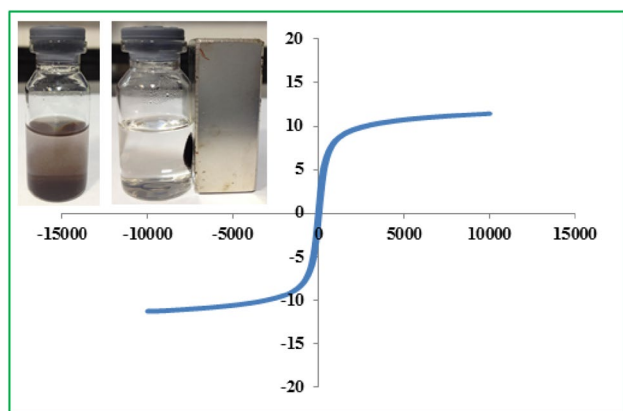


**Fig. 9** Room temperature magnetization curve of recycled  $\text{NiFe}_2\text{O}_4@ \text{SiO}_2@ \text{CS-Pd}$  catalyst

absorption bands of fresh catalyst were observed in XRD pattern and FT-IR spectrum of recycled catalyst, respectively. Therefore, results confirm that the catalyst retains its main structure during Suzuki coupling reactions.

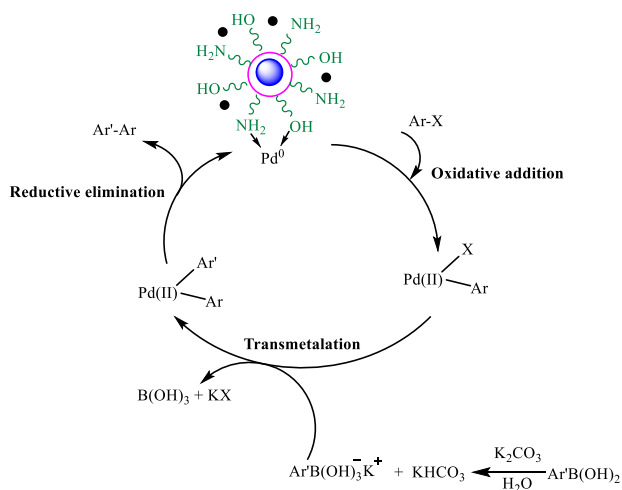
The magnetic properties investigation of the recycled catalyst showed that the magnetic intensity does not change after the 3 run (Fig. 9). These results indicate that the amount of palladium leaching is very low. Metal leaching will increase the amount of magnetic material per gram and so the magnetic intensity will increase.

To show the merit of the present work, we compared the results of  $\text{NiFe}_2\text{O}_4@ \text{SiO}_2@ \text{CS-Pd}$  with the previously reported catalyst systems in the synthesis of biphenyl via cross-coupling of bromobenzene with phenylboronic acid (Table 3). The results obtained with this catalytic system are superior to others, so that it gave a better yield in shorter time with lower loading of palladium catalyst under mild reaction conditions.

The mechanism of the Suzuki coupling reaction is presented in Scheme 2. Oxidative addition, transmetalation and reductive elimination are the three main steps in this coupling reaction [63]. The catalytic cycle begins with the oxidative addition of the aryl halide to Pd(0) and aryl palladium (II) intermediate formation ( $\text{Ar-Pd(II)-X}$ ). In transmetalation step, arylboronic acid which is activated by base reacts with aryl palladium (II) complex. Finally, reductive elimination of  $\text{Ar-Pd(II)-Ar}$  intermediate produces the desired coupling products.

**Table 3** Comparison results of NiFe<sub>2</sub>O<sub>4</sub>@SiO<sub>2</sub>-CS-Pd with other catalysts for the coupling of bromobenzene with phenylboronic acid

Entry	Catalyst	(mol%)	Solvent	Time	Yield (%)	Refs.
1	Pd-Fe <sub>3</sub> O <sub>4</sub> heterodimer nanocrystal catalyst	1	Reflux DMF/H <sub>2</sub> O	24 h	81	[56]
2	Pd <sup>0</sup> /mesoporous NiFe <sub>2</sub> O <sub>4</sub> -300	0.08	NMP/H <sub>2</sub> O, 80 °C	12 h	97	[57]
3	Pd/NiFe <sub>2</sub> O <sub>4</sub>	0.1	DMF/H <sub>2</sub> O, 90 °C	1 h	69	[58]
		1		30 min	98	
4	Pd-CS@SiO <sub>2</sub>	1	EtOH 95%, 80 °C	1 h	90	[15]
5	Pd NPs@chitosan	0.1	TBAB, 90 °C	5 h	97	[59]
6	CS-g-mPEG350 Pd (0)	0.5	H <sub>2</sub> O, 100 °C	2 h	79	[33]
7	Cell-Pd(0)	0.3	TBAB, H <sub>2</sub> O, 100 °C	6 h	92	[60]
8	Pd@Al <sub>2</sub> O <sub>3</sub> -CELL	1	H <sub>2</sub> O/DMF, 80 °C	1.5 h	95	[61]
9	Cell-AMP-Pd	0.75	EtOH 50%, 50 °C	3.5 h	91	[62]
10	NiFe <sub>2</sub> O <sub>4</sub> @SiO <sub>2</sub> -CS-Pd	8 × 10 <sup>-5</sup>	EtOH 95%, 75 °C	5 min	98	Our

**Scheme 2** Mechanism of the Suzuki cross-coupling reaction by NiFe<sub>2</sub>O<sub>4</sub>@SiO<sub>2</sub>@CS-Pd catalyst

## Conclusion

In conclusion, NiFe<sub>2</sub>O<sub>4</sub>@SiO<sub>2</sub>@CS-Pd nanocatalyst with a high magnetic and excellent dispersibility was prepared from NiFe<sub>2</sub>O<sub>4</sub>@SiO<sub>2</sub> with sequential attachment of chitosan, followed by treatment with an ethanolic solution of palladium chloride. The catalytic activities of this novel magnetic palladium catalyst were investigated in Suzuki coupling reaction. Moreover, the catalyst can be conveniently separated and recovered from the reaction system by a magnet and can be reused for at least nine times without noticeable loss of its activity. The generation of nanoparticles without addition of any external reducing agents, stability toward air and humidity, easy handling and recycle ability are some unique features of this catalytic system. We expect that this novel heterogeneous magnetic nanocatalyst has more wide applications in palladium catalyzed reactions.

**Acknowledgements** We gratefully acknowledge the partial financial support received from the research council of Alzahra University.

## References

- Á. Molnár, A. Papp, *Catal. Sci. Technol.* **4**, 295 (2014)
- A. Dewan, P. Bharali, U. Bora, A.J. Thakur, *RSC. Adv.* **6**, 11758 (2016)
- S. Keshipour, N. Kalam Khalteh, *Appl. Organomet. Chem.* **30**, 653 (2016)
- E. Guibal, *Sep. Purif. Technol.* **38**, 43 (2004)
- E. Guibal, *Prog. Polym. Sci.* **30**, 71 (2005)
- M. Lee, B.Y. Chen, W. Den, *Appl. Sci.* **5**, 1272 (2015)
- G.Z. Kyzas, D.N. Bikiaris, *Mar. Drugs.* **13**, 312 (2015)
- A. El Kadib, *Chem. Sus. Chem.* **8**, 217 (2015)
- A. Pestov, S. Bratskaya, *Molecules* **21**, 330 (2016)
- J. Zhou, Z. Dong, H. Yang, Z. Shi, X. Zhou, R. Li, *Appl. Surf. Sci.* **279**, 360 (2013)
- S. Keshipour, F. Ahmadi, B. Seyyedi, *Cellulose* **24**, 1455 (2017)
- M. Chichigrovsky, A. Primo, P. Gonzalez, K. Molvinger, M. Robitzer, F. Quignard, F. Taran, *Angew. Chem.* **121**, 6030 (2009)
- S. Kumar, N. Singhal, R.K. Singh, P. Gupta, R. Singh, S.L. Jain, *Dalton Trans.* **44**, 11860 (2015)
- A. Affrose, P. Suresh, I. Abulkalam Azath, K. Pitchumani, *RSC. Adv.* **5**, 27533 (2015)
- S. Jadhav, A. Kumbhar, R. Salunkhe, *Appl. Organomet. Chem.* **29**, 339 (2015)
- T. Baran, I. Sargin, M. Kaya, A. Menteş, *Carbohydr. Polym.* **152**, 181 (2016)
- D. Lv, M. Zhang, *Molecules* **22**, 150 (2017)
- Y. Liu, C. Peng, S. Linyong, Y. Fang, *Radiat. Phys. Chem.* **76**, 1165 (2007)
- H. Huang, X. Yang, *Carbohydr. Res.* **339**, 2627 (2004)
- M. Adlim, M.A. Bakar, K.Y. Liew, J. Ismail, *J. Mol. Catal. A Chem.* **212**, 141 (2004)
- E. Guibal, T. Vincent, *J. Environ. Manage* **71**, 15 (2004)
- Y.N. Gavhane, A.S. Gurav, A.V. Yadav, *Int J. Res. Pharm. Biomed. Sci.* **4**, 312 (2013)
- G. Li, Y. Jiang, K. Huang, P. Ding, J. Chen, *J. Alloys Compd.* **466**, 451 (2008)
- L. Fan, C.N. Luo, M. Sun, X.J. Li, *Colloids Surf. B* **95**, 42 (2012)
- L. Li, L. Fan, C. Luo, H. Duan, X. Wang, *RSC Adv.* **4**, 24679 (2014)

26. J. Wencel-Delord, A. Panossian, F.R. Leroux, F. Colobert, *Chem. Soc. Rev.* **44**, 3418 (2015)
27. G. Bringmann, T. Gulder, T.A.M. Gulder, M. Breuning, *Chem. Rev.* **111**, 563 (2011)
28. F.M. Meyer, J.C. Collins, B.P. Borin, J. Bradow, S. Liras, C. Limberakis, A.M. Mathiowetz, L. Philippe, D. Price, K. Song, K. James, *J. Organ. Chem.* **7**, 3099 (2012)
29. S. Kappaun, C. Slugovc, E.J.W. List, *Int. J. Mol. Sci.* **9**, 1527 (2008)
30. J. Bao, W.D. Wulff, A.L. Rheingold, *J. Am. Chem. Soc.* **115**, 3814 (1993)
31. N. Miyaura, A. Suzuki, *Chem. Rev.* **95**, 2457 (1995)
32. S.S. Yi, D.H. Lee, E. Sin, Y.S. Lee, *Tetrahedron Lett.* **48**, 6771 (2007)
33. E. Sin, S.S. Yi, Y.S. Lee, *J. Mol. Catal. A Chem.* **315**, 99 (2010)
34. J.J.E. Hardy, S. Hubert, D.J. Macquarrie, A.J. Wilson, *Green Chem.* **6**, 53 (2004)
35. T. Baran, *Hacet. J. Biol. Chem.* **44**, 307 (2016)
36. A.R. Hajipour, E. Boostani, F. Mohammadsaleh, *RSC Adv.* **5**, 24742 (2015)
37. A. Naghipour, A. Fakhri, *Catal. Commun.* **73**, 39 (2016)
38. K. Maaz, S. Karim, A. Mumtaz, S.K. Hasanain, J. Liu, J.L. Duan, *J. Magn. Magn. Mater.* **321**, 1838 (2009)
39. A. Chaudhuri, M. Mandal, K. Mandal, *J. Alloys Compd.* **487**, 698 (2009)
40. S. Mohammadi-Samani, R. Miri, M. Salmanpour, N. Khalighian, S. Sotoudeh, N. Erfani, *Res. Pharm. Sci.* **8**, 25 (2013)
41. W.T. Liu, Y. Yang, P.H. Shen, X.J. Gao, S.Q. He, H. Liu, C.S. Zhu, *Express Polym. Lett.* **9**, 1068 (2015)
42. A. Chaudhuri, M. Mandal, K. Mandal, *J. Alloys Compd.* **487**, 698 (2009)
43. A. Khojastehnezhad, M. Rahimizadeh, F. Moeinpour, H. Eshghi, M. Bakavoli, *C. R. Chimie* **17**, 459 (2014)
44. F. Abrishami, M. Ebrahimikia, F. Rafiee, *Appl. Organomet. Chem.* **29**, 339 (2015)
45. T. Ahmad, H. Bae, Y. Iqbal, I. Rhee, S. Hong, Y. Chang, J. Lee, D. Sohn, *J. Magn. Magn. Mater.* **381**, 151 (2015)
46. S. Ramezani, A. Ghazitabar, S.K. Sadrnezhad, *J. Iran. Chem. Soc.* **13**, 2069 (2016)
47. R. Kaiser, G. Miskolczy, *J. Appl. Phys.* **41**, 1064 (1970)
48. B. Mu, T. Li, J. Li, Y. Wu, *J. Organomet. Chem.* **693**, 1243 (2008)
49. T. Mino, Y. Shirae, M. Sakamoto, T. Fujita, *J. Organ. Chem.* **70**, 2191 (2005)
50. X. Li, W. Chen, H. Chang, Z. Shao, W. Wei, *Synthesis* **46**, 1593 (2014)
51. Q. Zhang, H. Su, J. Luo, Y. Wei, *Catal. Sci. Technol.* **3**, 235 (2013)
52. B. Karimi, P. Fadavi Akhavan, *Chem. Commun.* **47**, 7686 (2011)
53. N. Iranpoor, H. Firouzabadi, R. Azadi, *J. Organomet. Chem.* **693**, 2469 (2008)
54. F. Rafiee, N. Mehdizadeh, *Catal. Lett.* **148**, 1345 (2018)
55. C.K. Bradsher, F.C. Brown, H.K. Porter, *J. Am. Chem. Soc.* **76**, 2357 (1954)
56. Y. Jang, J. Chung, S. Kim, S.W. Jun, B.H. Kim, D.W. Lee, B.M. Kim, T. Hyeon, *Phys. Chem. Chem. Phys.* **13**, 2512 (2011)
57. Z. Gao, Y. Feng, F. Cui, Z. Hua, J. Zhou, Y. Zhu, J. Shi, *J. Mol. Catal. A Chem.* **336**, 51 (2011)
58. S.R. Borhade, S.B. Waghmode, *Beilstein. J. Organ. Chem.* **7**, 310 (2011)
59. P. Cotugno, M. Casiello, A. Nacci, P. Mastroilli, M.M. Dell'Anna, A. Monopoli, *J. Organomet. Chem.* **752**, 1 (2014)
60. N. Jamwal, R.K. Sodhi, P. Gupta, S. Paul, *Int. J. Biol. Macromol.* **49**, 930 (2011)
61. A. Kumbhar, S. Jadhav, S. Kamble, G. Rashinkar, R. Salunkhe, *Tetrahedron Lett.* **54**, 1331 (2013)
62. P. Hu, Y. Dong, X. Wu, Y. Wei, *Front Chem. Sci. Eng.* **10**, 389 (2016)
63. K. Matos, J.A. Soderquist, *J. Organ. Chem.* **63**, 461 (1998)